FERMILAB-CONF-75-140-E

J/ψ Production by Neutrons and Photons and Dimuon Continuum *

Wonyong Lee
Columbia University, New York, N.Y. 10027

I will talk about the recent results on J/ψ production[1] in reactions induced by neutrons and photons at Fermilab. The experiment was carried out by a group of physicists from Columbia, Cornell, Fermilab, Hawaii and Illinois.[2] Let me first talk about the photoproduction experiment.

The photons are obtained from a 0-mr neutral neutral beam which is produced by the interactions of 300/380 GeV protons in a 30.5 cm Be target. The γ-to-n ratio is improved by a factor of roughly 200 above the γ-to-n ratio at production by passing the beam through 34 m of liquid D_2. With the primary proton energy of 300 GeV, the photon spectrum at the experimental target is shown in Fig. 1.

The detector, which is shown in Fig. 2, consists of a multi-wire proportional chamber magnetic spectrometer and a particle identifier. The spectrometer magnet M2, which has a field integral of 20 kG m, bends the trajectories of charged particles vertically. The magnet aperture, which is 61 cm high and 40.6 cm wide, determines the acceptance of the spectrometer.

Scintillation detectors T, AB and AW, as shown in Fig. 3, cover most of solid angle not covered by multiwire proportional chambers. The counters T are placed to detect recoiling protons and the counters AB and AW covered forward cone.

The particle identifier consists of an electron (and photon) calorimeter, a hadron calorimeter, and a muon identifier, as shown in Fig. 4. The electron calorimeter is made up of an upstream and a downstream shower-counter hodoscope. Each hodoscope is split into two identical halves which are separated horizontally from each other by 10 cm, in order to allow the beam and the copiously produced e^+e^- pairs to pass through. Each upstream hodoscope counter contains six layers of lead and plastic, and each counter of

Talk presented at SLAC Summer Institute (July 28-30, 1975.)

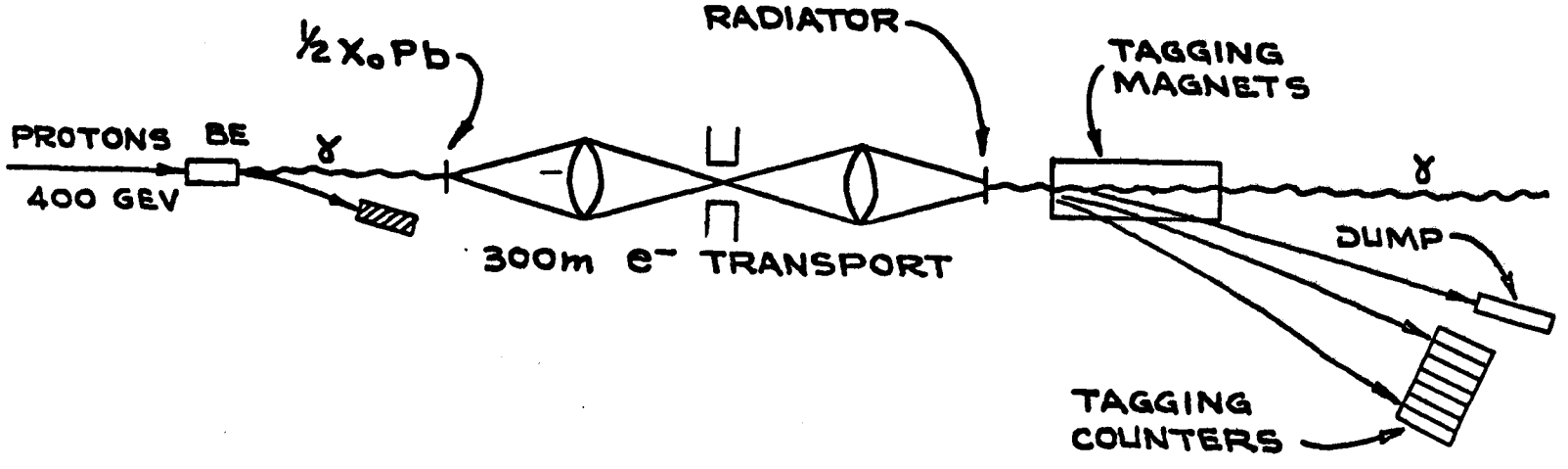

Fig. 1 Layout of the electron/tagged photon beam

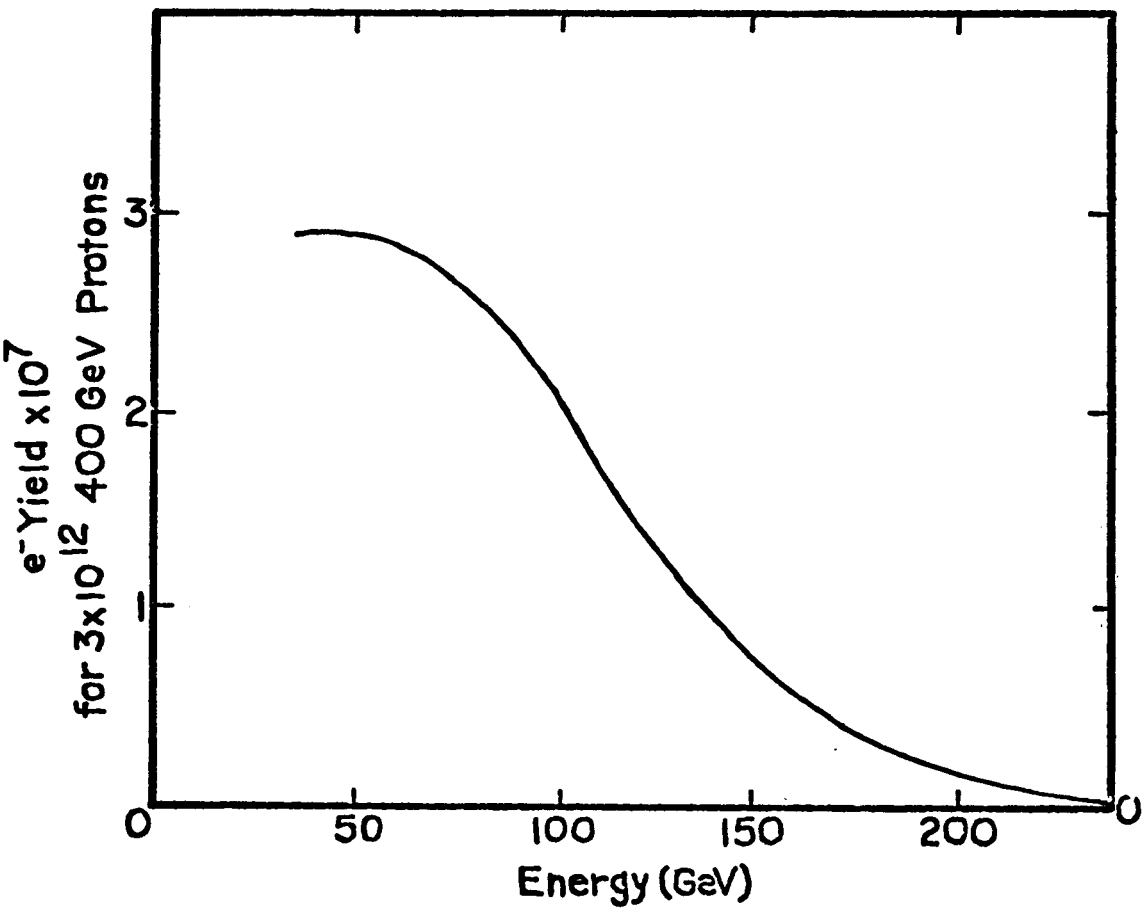

Fig. 2 Electron energy spectrum with 300 GeV proton incident on the Be target

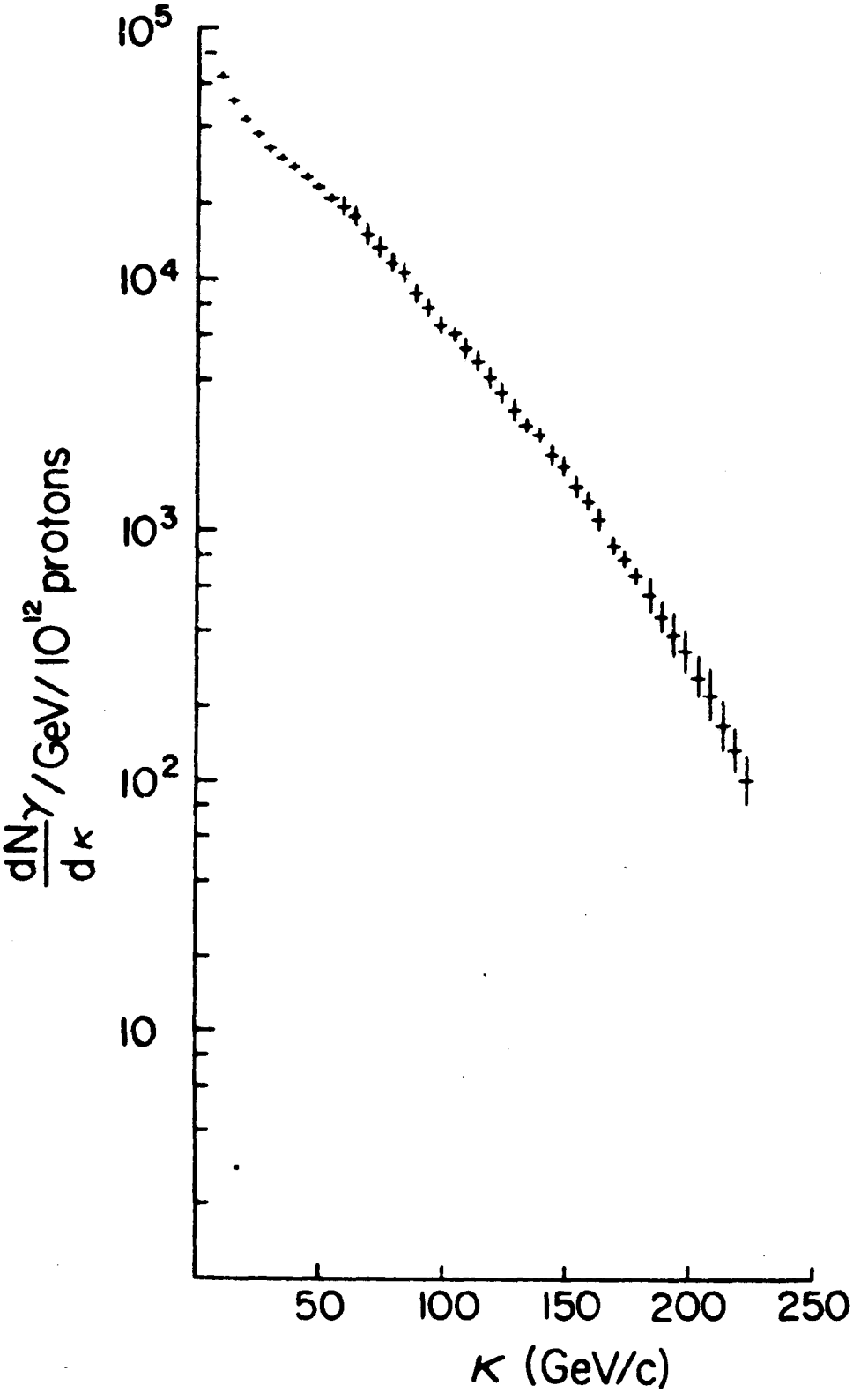

Fig. 3 Photon energy spectrum at photon target with the cryostat filled with liquid D2

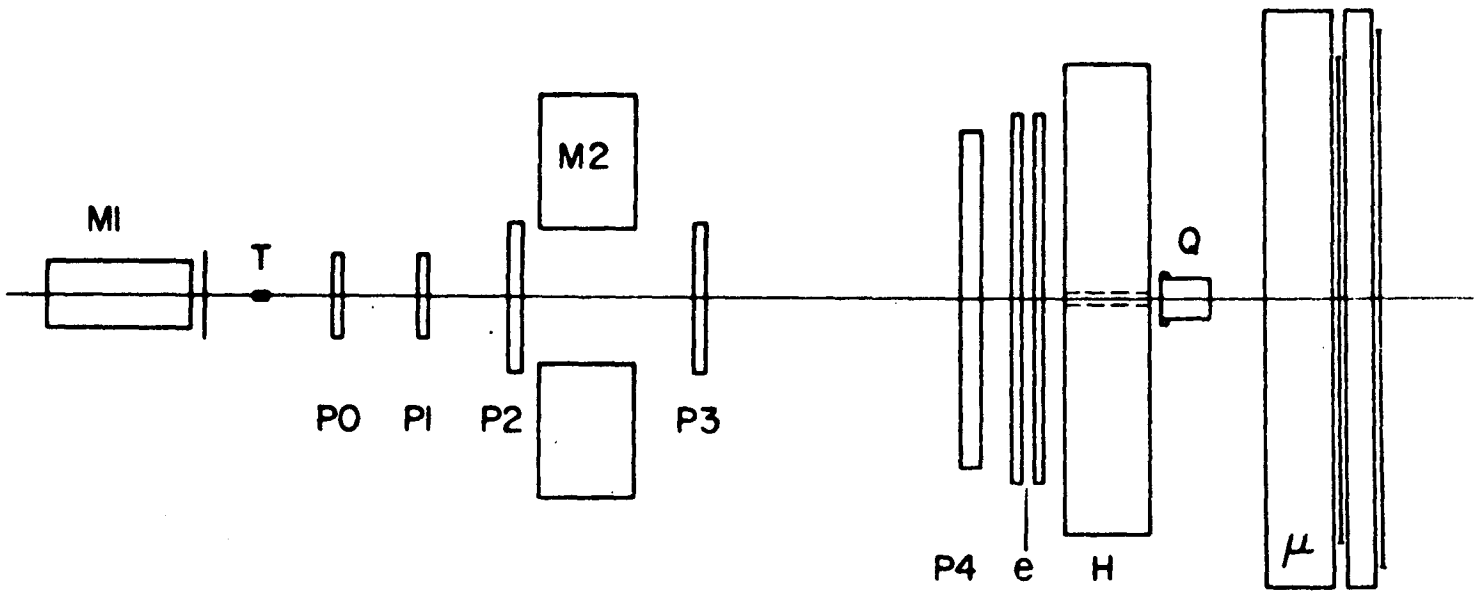

Fig. 4 Layout of detectors in experimental enclosure

the downstream hodoscope contains sixteen layers of lead and plastic. A layer is composed of a 4.8-mm thick plastic scintillator and a 6.3-mm thick Pb sheet.

The hadron calorimeter consists of twenty-four 4.45-cm steel plates interleaved with 6.3-mm sheets of plastic scintillator. A 15-cm square hole allows the beam to pass through the calorimeter. The muon identifier consists of a steel shield which is 60-cm thick, and an 18-element vertical, 22-element horizontal scintillation counter hodoscope.

The photon beam intensity is monitored continuously by a 26-radiation length Wilson quantameter. At regular intervals, the photon spectrum is determined by measuring the total momentum of e^+e^- pairs produced in a 0.04-radiation length lead target. During the calibration runs, the target is inserted in the photon beam in front of a horizontally bending dipole magnet M1 which opens the e^+e^- pairs so that their momentum can be measured in the multiwire proportional chamber spectrometer.

Events which have two or more tracks and which satisfy any of the following requirements are recorded on magnetic tape: Two or more muons in the muon identifier, two or more electrons in the electron calorimeter, one electron and one muon, and finally, any event which deposits more than a preset amount of energy in the hadron calorimeter.

For each event, all possible tracks are reconstructed from the multiwire proportional chamber hits.

Let me now discuss the important characteristics of events which possess a dimuon in the final states.

Each track is extrapolated back to each plane of muon counters, and a circle with a radius 2.5 times the expected deviation due to multiple scattering is computed. Any muon counter with a hit which overlaps this circle is considered to be correlated with the track. A "muon" track is required to have correlated hits in both muon counter planes.

The sample of all events with two muon tracks is extracted. The paths of the two muons are extrapolated back to the target to determine if the pair came from a single

point within the target. The distance of closest approach, the shortest line segment connecting the two tracks in front of the magnet, is required to be less than 2.5 mm. The vertex of the event is defined to be the midpoint of this line segment. It must be located within 20 cm of the target along the beam direction.

The momentum of each track is computed assuming that the magnetic field is uniform. The momentum resolution in the limit of a uniform field is calculated to be $\delta P/P = \pm 0.03$ (P/100 GeV/c).

The raw mass spectrum for a sample of 60 events with momenta greater than 80 GeV/c is shown in Fig. 5. The two principal features of these data, which can be seen readily, are a preponderance of events at low mass, characteristic of muon-pair production by the Bethe-Heitler mechanism, and a peak at 3.1 GeV/c^2. It should be pointed out that this sample was not restricted to two track events. The width is consistent with our experimental resolution. The data were also taken with the photon target closer to the magnet to obtain events with momenta between 50 GeV and above. The combined data sample, which has 102 events, was used to produce the t distribution shown in Fig. 6. The t distribution for the $\pi^+\pi^-$ final state with a mass of the rho meson can be fitted very well with the sum of two exponentials, one with a slope of ~ 60 GeV^{-2} which is characteristic of the coherent scattering from the Be nucleus, and the other with a slope of ~ 10 GeV^{-2} which is characteristic of scattering from single nucleons in Be. One can also see these same features in the t distribution of the 3.1 GeV/c^2 resonance. The fitted value of the slope is approximately $\sim$ fifty and $\sim$ two 1 GeV^2.

There are two principal sources of background in the determination of the ψ cross section.

First, we must determine what fraction of the events are produced by hadrons in our beam. Our measured cross section for ψ by neutrons in this beam and the known ratio of photons to neutrons allow us to determine that the number of events in this experiment induced by neutrons is consistent with zero.

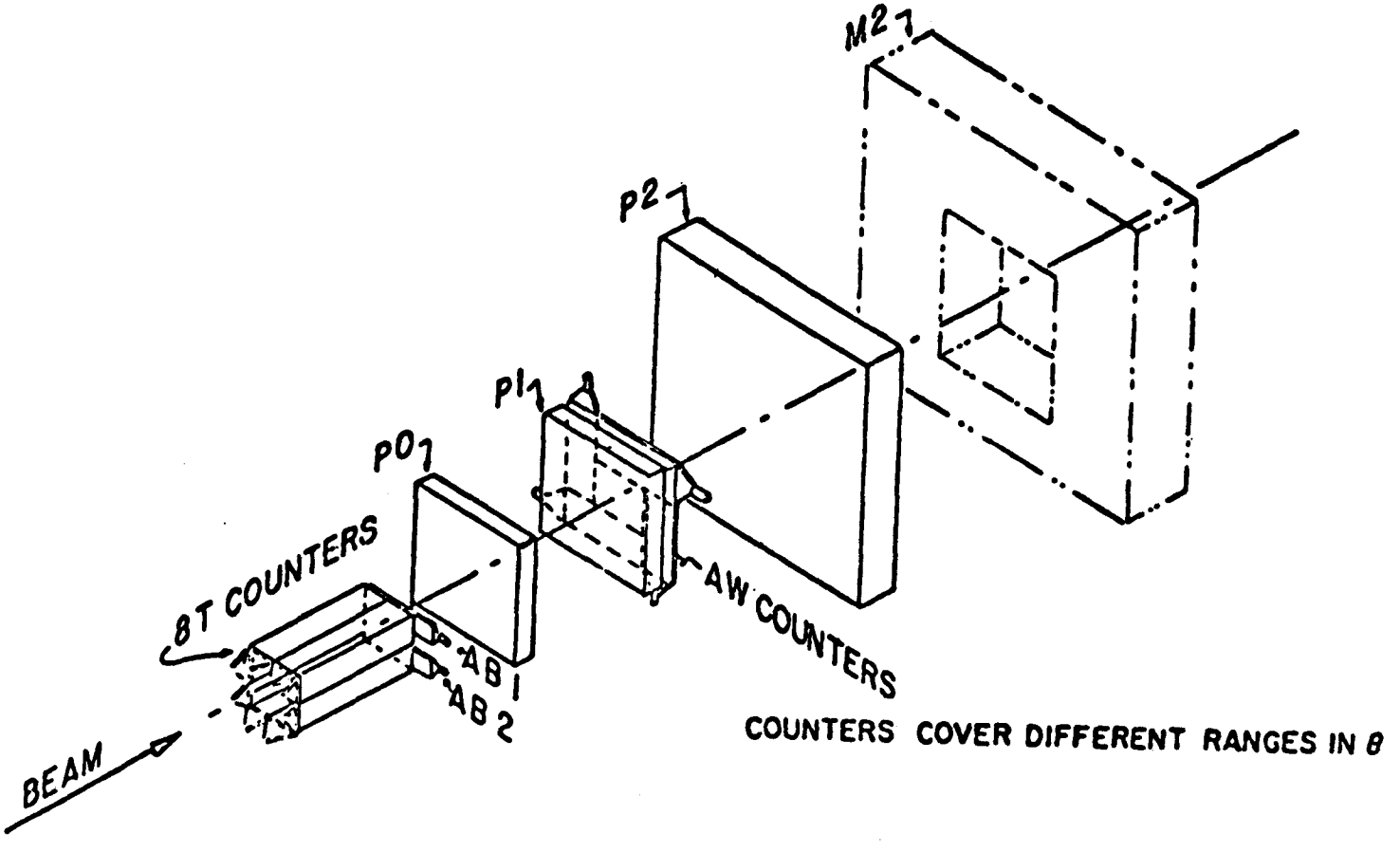

Fig. 5 Layout of scintillation detectors near the photon target

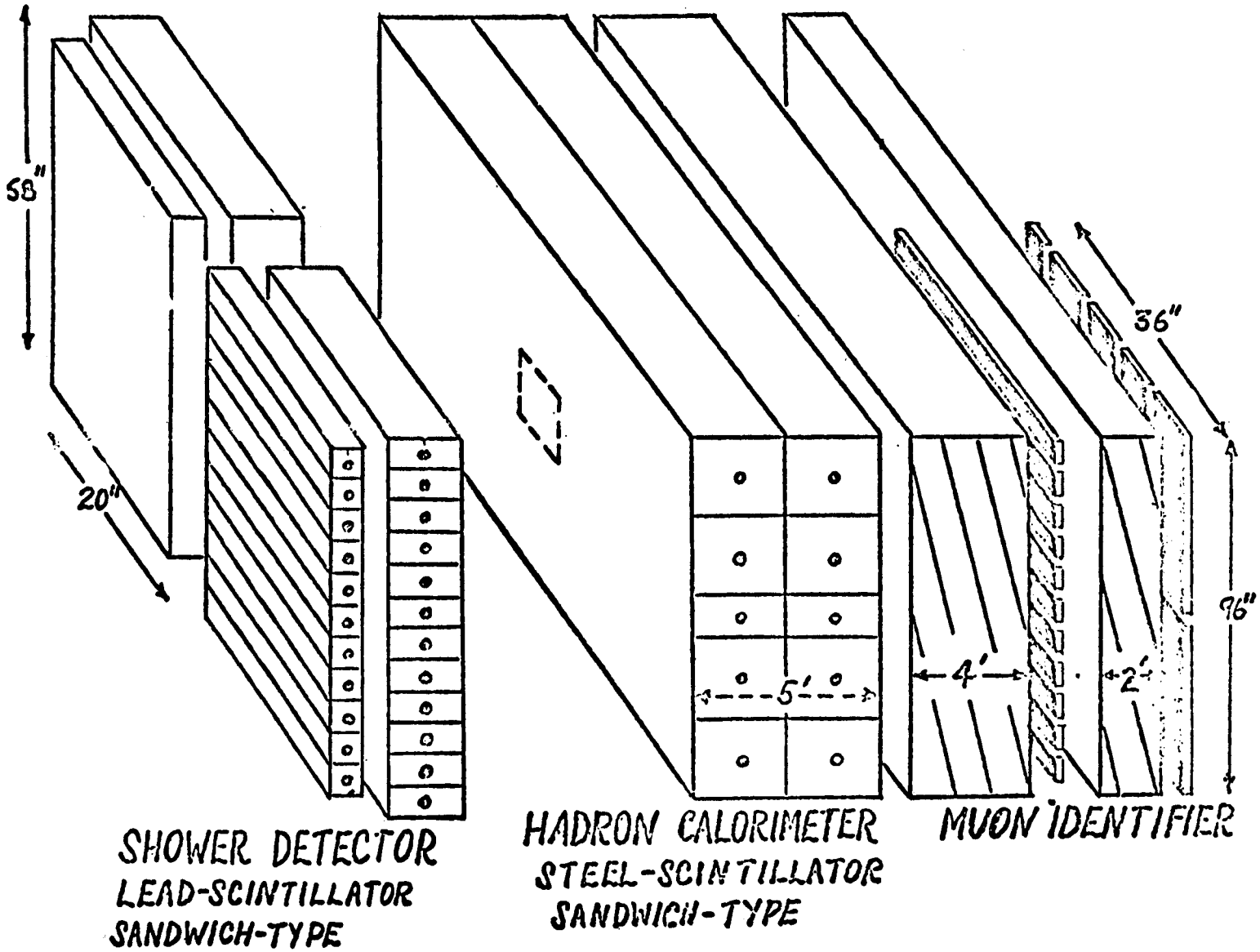

Fig. 6 Layout of particle identifier

The other source of background is the photoproduction of the $\psi'(3700)$ and its decay into $\psi(3100)$ + X with the subsequent decay of the $\psi(3100)$ into two muons.

We have observed two events which are

$$\gamma + Be \rightarrow \psi'(3700) + ...$$
$$\rightarrow \psi(3100) + \pi^+ + \pi^-$$
$$\rightarrow \mu^+\mu^- .$$

Based on Monte Carlo calculations, we place an upper limit from this source to be 15% or less.

Based on 102 events and correcting for geometric acceptance and electronic deadtime, we measure:

$$\sigma(\gamma+Be \rightarrow \psi+....)B(\psi \rightarrow \mu^+\mu^-) = 20 \pm 5 \text{ nb/nucleus.}$$

We also determine:

$$\frac{d\sigma}{dt}(\gamma+N \rightarrow \psi+N)\Big|_{t=0} = 55 \pm 24 \text{ nb/GeV}^2 .$$

Here N is a nucleon. This cross section was determined by first determining the differential cross section at t = 0 $\frac{d\sigma}{dt}|(\gamma+Be \rightarrow \psi+Be)|_{t=0}$ and then dividing by A^2, A being the atomic number of Be nucleus.

If we assume the validity of vector dominance and that the forward scattering amplitude is purely imaginary, we obtain for the ψN total cross section

$$\sigma(\psi N) \simeq 1 \text{ mb.}$$

While these assumptions are reasonable for other vector meson photoproduction processes, we have no evidence for their validity in this case.

In order to determine ψN interaction strength without making the above assumptions, we have made a preliminary study of the A dependence of the photoproduction cross section of the ψ. Limiting the ψ events to the small momentum transfer region ($-t < 0.07$ GeV^2), we observed 10 $\psi \rightarrow \mu^+\mu^-$ and e^+e^- events in the reaction $\gamma+Pb \rightarrow \psi+....$. We would expect to see 11 events if $\sigma(\psi N) = 0$ mb, 5 if $\sigma(\psi N) = 15$ mb, and 4 if $\sigma(\psi N) = 30$ mb. Obviously, we cannot draw any conclusion about the magnitude of $\sigma(\psi N)$ based on our present data. In these calculations, we have used 2.71 fm for the Be radius and 5.66 fm for the Pb nucleus.

Conclusions:

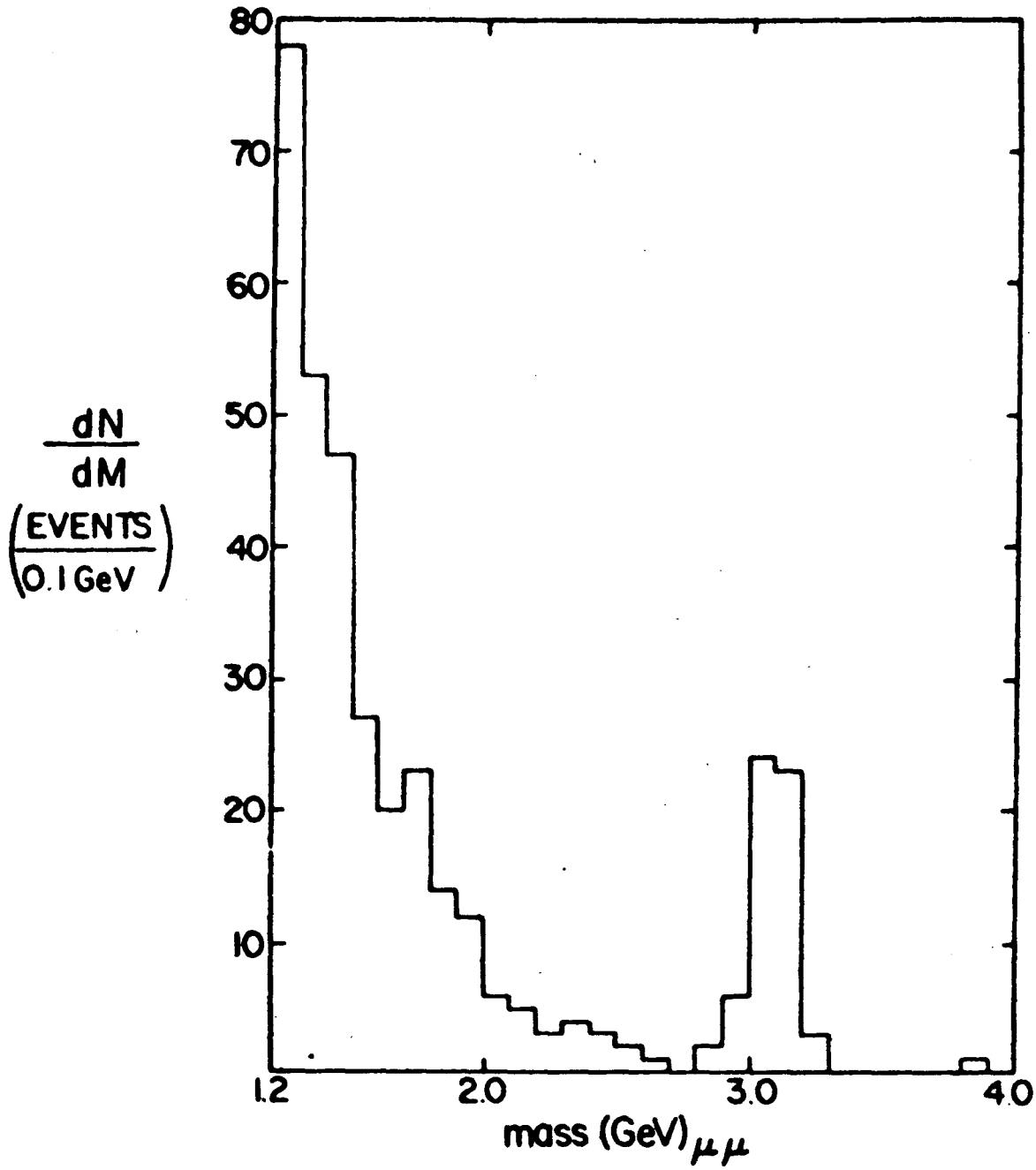

Fig. 7 Dimuon invariant mass distribution observed above 1.2 GeV

1) We observed photoproduction of $\psi(3100)$ and $\psi(3700)$.
2) The $\psi(3100)$ is photoproduced diffractively on the Be nucleus.
3) We find $\sigma(\psi N) \sim 1.0$ mb if we assume vector dominance and that the forward scattering amplitude is purely imaginary.

We now turn to the neutron experiment.

The neutron experiment used the same detectors but differed from the photon experiment in two respects. First, the 34 m of liquid deuterium was emptied and 3.8 cm of Pb was placed upstream in the neutral beam line, thereby selectively attenuating the photons. The neutral beam was then predominantly neutrons. Secondly, the multiwire proportional chamber, P1, was moved 75 cm downstream in order to insert an absorber, 61 cm of Be followed by 183 cm of Fe, into the beam. It attenuates reaction products other than muons and reduces the decay path for pions produced in the target to 150 cm.

The first 60 cm of neutron absorber is subdivided into twelve layers of 6-mm thick plastic scintillator, interspersed with 4.4-cm thick sheets of steel, which are viewed by a single phototube. This calorimeter was calibrated in a 50-GeV pion beam and found to have a resolution of $\pm$ 25%. It is used at low intensities to determine the incident neutron energy spectrum.

Figure 8 shows the energy spectrum unfolded from the pulse height distribution of the calorimeter. The spectrum of photons surviving the 3.8 cm of Pb is also shown for the corresponding number of proton interactions in the primary target.

Because of the additional absorber, analysis of these experimental data differs from that described earlier. Only four proportional chambers downstream of the absorbers are used to measure the direction and momentum of charged particles emerging from the absorber. Since muons typically lose more than 3 GeV and suffer multiple scattering with about 170 MeV/c rms transverse momentum in the absorber, the dimuon mass resolution is worse. The neutron analysis is checked by restoring the photon beam and observing a comparable number of photoproduced dimuons with the absorber still in place.

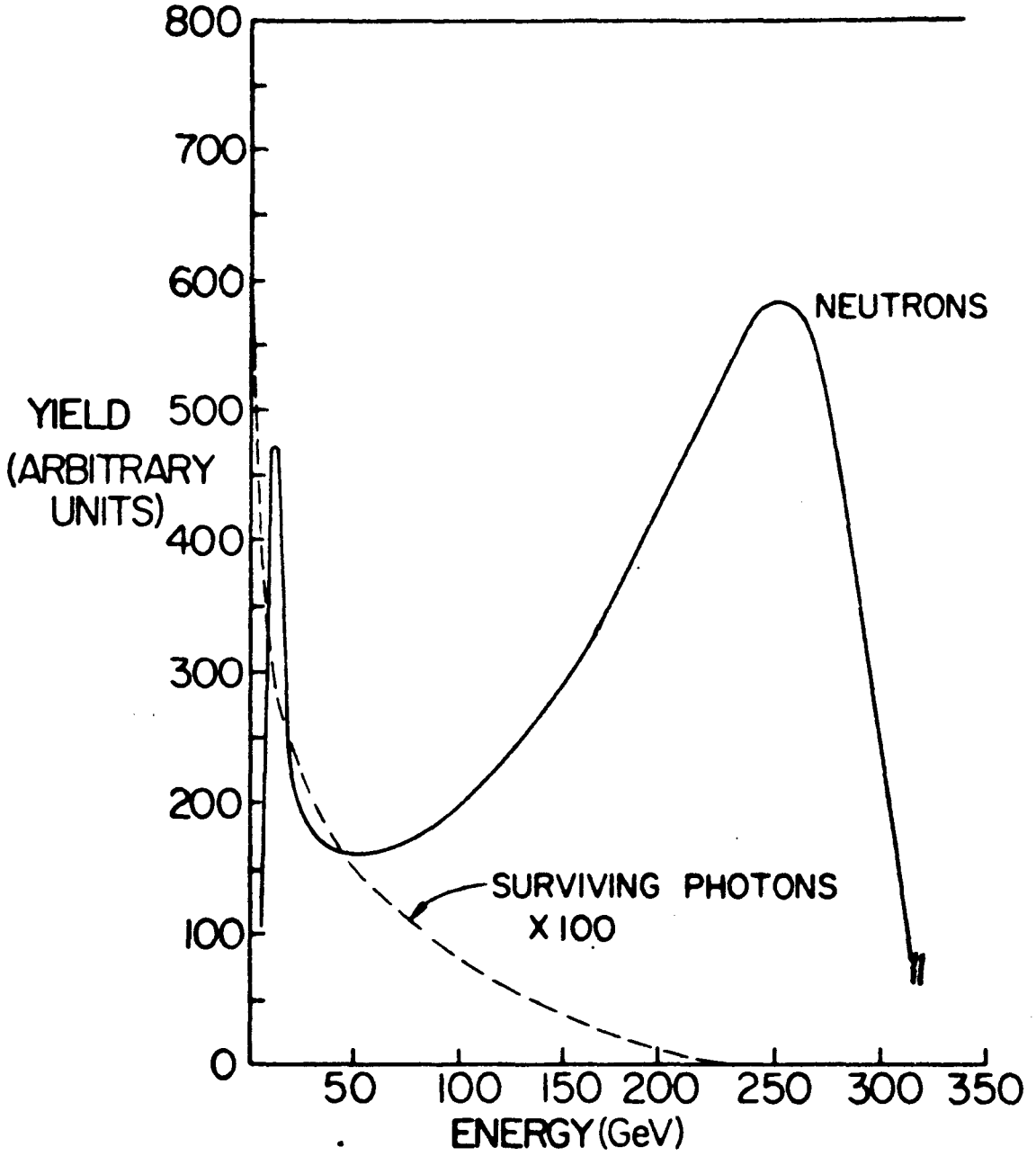

Fig. 8 Neutron energy spectrum (raw distribution of neutron calorimeter pulse height) with the spectrum of surviving photons superimposed

Thus, by comparing to the photoproduced dimuon data, we directly measure the effect of the absorber on our resolution in the kinematical variables.

To calculate the dimuon mass $M_{\mu\mu}$, we use the high energy, small angle formula

$$M_{\mu\mu}^2 = m^2(2 + \frac{E_1}{E_2} + \frac{E_2}{E_1}) + E_1E_2\theta_{12}^2 ,$$

where m is the muon mass, E_1 and E_2 are the muon energies corrected for loss in the absorber, and θ_{12} is the opening angle between the two muons. If the production point is known, the measurement of θ_{12} least affected by multiple scattering is obtained by dividing the apparent separation of the two muons when they are extrapolated back to the plane 50 cm downstream from the middle of the Fe absorber by the distance from the production point to that plane. Mistakenly assuming that the dimuon originating in the absorber had been produced in the target would seriously underestimate the dimuon mass.

The invariant mass distribution calculated for oppositely charged dimuons of total energy greater than 70 GeV is shown in Fig. 9. We see clear peaks at 0.76 and 3.1 GeV/c^2 with widths consistent with the expected experimental resolution. There are 43 events in the 3.1 GeV/c^2 region. To be included in the mass plot, the reconstructed vectors must pass within 2.5 cm of one another when extrapolated to their point of closest approach and their mean transverse separation from the beam axis weighted by energy must be less than 7.5 cm at that point.

For dimuons of mass above 1 GeV, our resolution in the distance of closest approach is sufficient to separate pairs produced in the dump from those produced in the target. The large enhancement seen at the ρ mass in Fig. 9 clearly indicates ρ production in the target, but any ρ produced by interactions in the absorber would be lost in the continuous distribution at lower masses. Similarly, low mass dimuons produced in the target are indistinguishable from those produced in the dump by photons from π^o decay.

Figures 10a and b show the $P_\perp^2$ distribution of the dimuons in the two mass regions: $0.7 < M_{\mu\mu} < 0.85$ GeV/c^2 and the

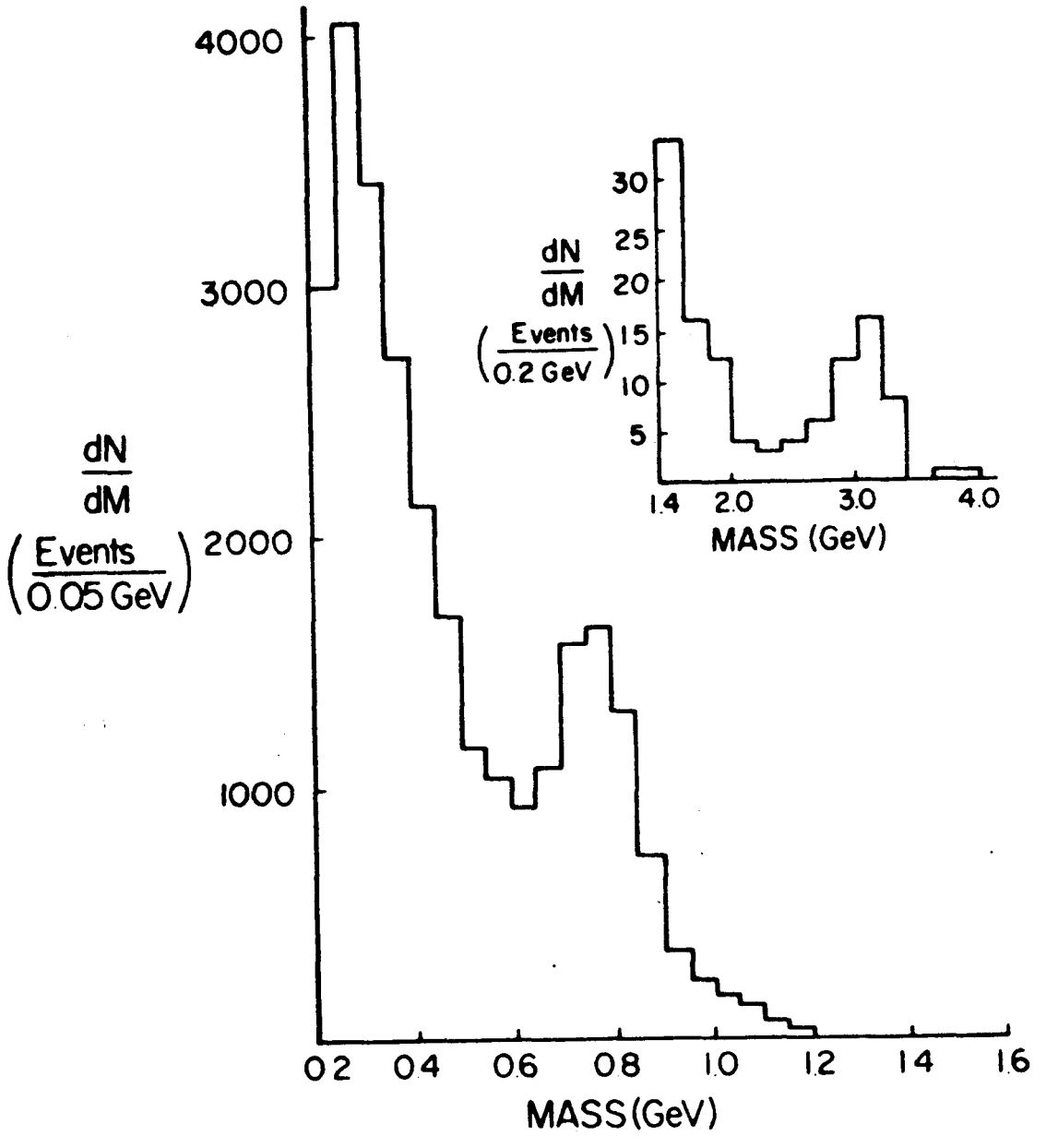

Fig. 9 Invariant-mass distribution of pairs of muons with opposite charge and total energy greater than 70 GeV

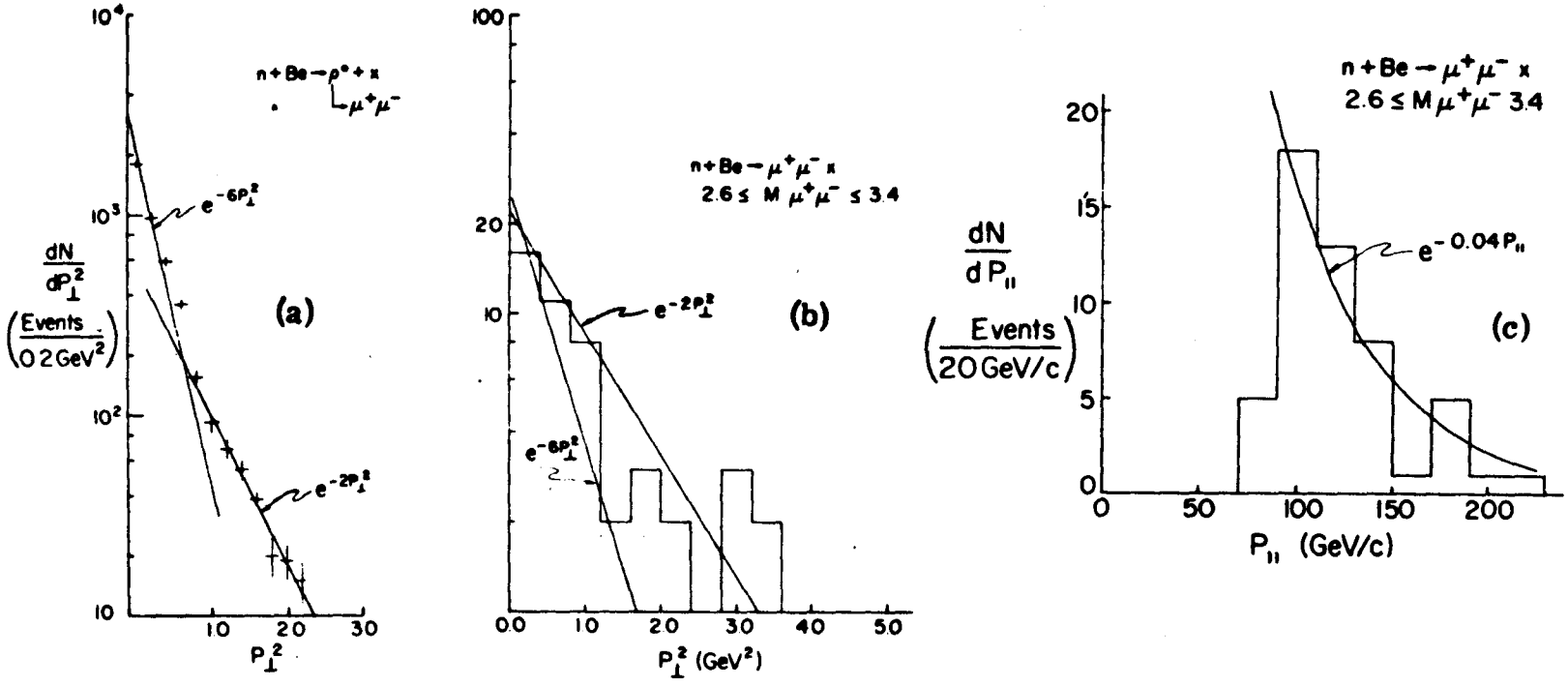

Fig. 10 Distributions for events in Fig. 9: (a) $P_\perp^2$ for $0.7 < M_{\mu\mu} < 0.85$ GeV/c^2; (b) $P_\perp^2$ and (c) $P_{||}$ for $2.6 < M_{\mu\mu} < 3.4$ GeV/c^2.

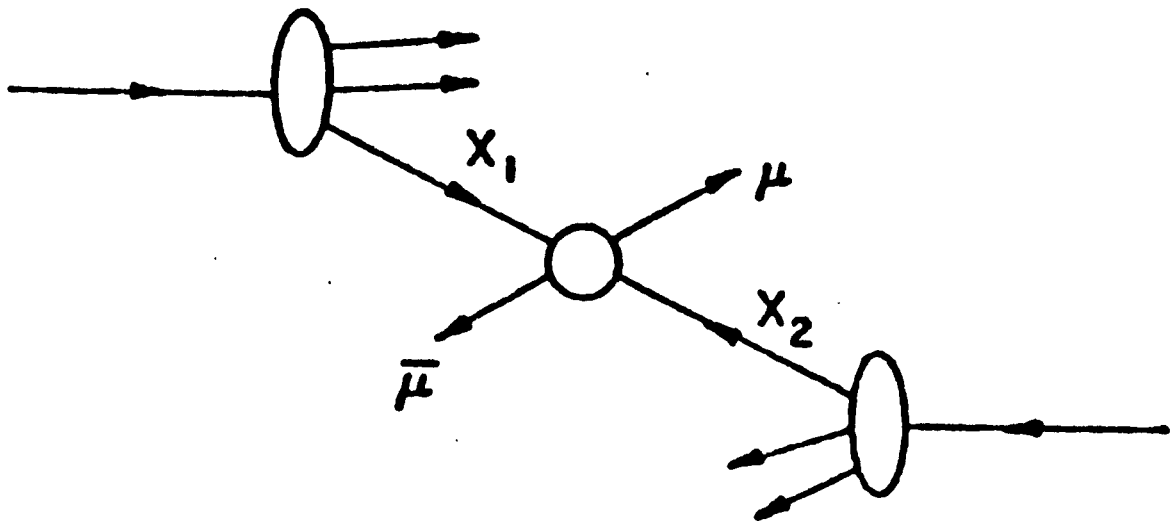

Fig. 11 The Drell-Yan mechanism for massive dimuon production

high mass region $2.6 < M_{\mu\mu}$. Note that the 3.1 GeV/c^2 object is produced with a considerably larger average value of $P_\perp^2$ than the ρ meson. We show the total momentum distribution of the dimuon in Fig. 10c.

We have compared our data with Monte Carlo simulations of events generated according to

$$d^2\sigma/dxdP_\perp^2 \propto \exp(-\alpha x)\exp(-\beta P_\perp^2) , \qquad (1)$$

where x is the ratio of the dimuon momentum to that of the incoming neutron in the laboratory.[3] The simulated events were then multiply scattered through the absorber and accepted by the apparatus. The resulting distributions for $P_\perp^2$ and $P_{||}$ are shown as the solid curves in Figs. 10a-c, for different values of β as indicated and for $\alpha = 10$.

The total cross section is calculated as follows: The total number of interactions was recorded. Each interaction was assumed to be 40 mb per nucleon. After correcting for electronic deadtime and geometric acceptance, we obtain

$$\sigma(n+Be \rightarrow J + X) \hookrightarrow \mu^+\mu^-$$
$$= 1.7 \times 10^{-33} \text{ cm}^2/\text{nucleon for } |x| > 0.32 .$$

In calculating geometric acceptance, we used $\alpha = 10$ and $\beta = 2$. We also calculated the acceptance for $\alpha = 7.5$, $\alpha = 12.5$, and $\beta = 1$, $\beta = 4$. On the basis of these calculations, we believe that we measured the total cross section to within a factor of 2.

If we extrapolate the equation (1) to $X_F = 0$, we obtain

$$\frac{d\sigma}{dy} = 7.5 \times 10^{-33} \text{ cm}^2$$

where y is rapidity. This is consistent with the cross section determined at the ISR.[4]

We now consider the dimuon continuum which we define in the mass region of $1.0 \leq M_{\mu\mu} < 2.4$ GeV[4] and we will compare our data with the Drell-Yan mechanism.[5]

The mechanism they considered for massive dimuon production is shown in Fig. 11. The pair is created by parton-antiparton annihilation when a parton (antiparton) moving to the right with a fraction x_1 of the nucleon momentum annihilates with an antiparton (parton) with a fraction x_2 of the nucleon momentum. They obtain

$$\frac{d\sigma}{dM^2 dP^*} = \frac{1}{3}\int \frac{dx_1}{x_1}\frac{dx_2}{x_2}\sum_i e_i^2[f_i(x_1)\bar{f}_1(x_2)+f_i(x_2)f_i(x_1)]$$

$$\frac{4\pi\alpha^2}{3M^2}\,\delta(M^2-x_1x_2S)\,\delta(P^*-\frac{\sqrt{s}}{2}(x_1-x_2))$$

where M = dimuon mass, P^* = dimuon longitudinal momentum, x_1, x_2 = longitudinal fractions of the incident partons i, e_i = parton charges, f_i = density of parton of type i.

The normalization of f_i is such that

$$\nu W_2(x) = \sum_i e_i^2[f_i(x)+\bar{f}_i(x)] \quad .$$

Our experiment measures only a small part of the kinematics available for the parton antiparton phase space. Typical values are:

$M^2 \sim 2\ (GeV)^2$ $\qquad$ $S \sim 620\ (GeV)^2$

$x_1 \sim 0.2$ $\qquad$ $x_2 \sim 10^{-2}$.

We can now approximate the kinematical region we observe by:

$$f_i(x_2) \approx \bar{f}_i(x_2) \approx f_i(0)$$

or using a value of $\nu W_2(0) = 1/3$, $f_i(0) \approx 1/4$, we then obtain

$$\frac{d\sigma}{dM^2 dP^*} = \frac{1}{12}\int \frac{dx_1}{x_1}\int \frac{dx_2}{x_2}\,\nu W_2(x_1)$$

$$\frac{4\pi\alpha^2}{3M^2}\,\delta(M^2-x_1x_2S)\,\delta(P^*-\frac{\sqrt{s}}{2}(x_1-x_2)) \quad .$$

This equation was then integrated with a $P_{\|}^{L} > 60$ GeV/c cutoff. A comparison of the model with the experimental data is shown in Fig. 6. Except for the low mass region where we see a possible ϕ^o production and the tail of the ρ^o peak, we are consistent within a factor of ~ 3 with the predictions of the model. Given the uncertainty of the normalization (a factor 2-3), the agreement is remarkable. It should be pointed out that the dimuon in this mass region could be produced due to an entirely different mechanism, such as $\rho' \to \mu^+\mu^-$.

I would like to thank my colleagues on these experiments.

* Research supported in part by the National Science Foundation.

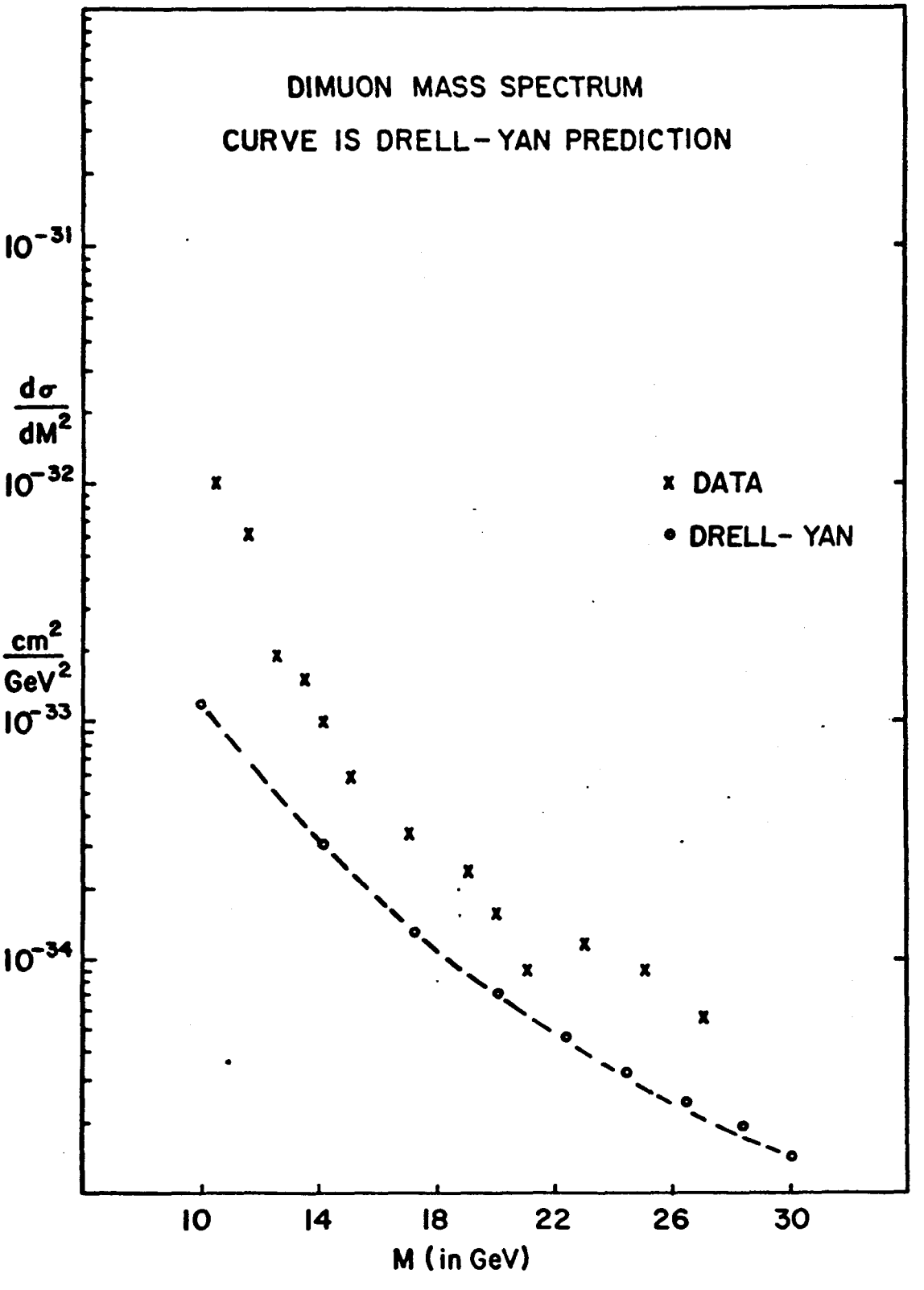
DIMUON MASS SPECTRUM
CURVE IS DRELL-YAN PREDICTION
10^{-31}
$\frac{d\sigma}{dM^2}$
10^{-32}
$\frac{cm^2}{GeV^2}$
10^{-33}
10^{-34}
x DATA
• DRELL-YAN
10
14
18
22
26
30
M (in GeV)

Fig. 12

References

1 J.J. Aubert et al, Phys. Rev. Letters 33, 1404 (1974). J.E. Augustin et al, Phys. Rev. Letters 33, 1406 (1974). We will call the 3.1 resonance J in hadron collisions and ψ in the photoproduction experiment.

2 B. Knapp, W. Lee, P. Leung, S.D. Smith, A. Wijangco, J. Knauer, D. Yount, D. Nease, J. Bronstein, R. Coleman, L. Cormell, G. Gladding, M. Gormley, R. Messner, T. O'Halloran, J. Sarracino, A. Wattenberg, D. Wheeler, M. Binkley, R. Orr, J. Peoples and L. Read, Phys. Rev. Letters 34, 1040, 34, 1044 (1975).

3 X is related to the usual c.m. X_F in the following manner,

$$X = \frac{1}{2}[X_F + (X_F^2 + \frac{4M_{\mu\mu}^2}{S})^{1/2}].$$

Note that $X \approx X_F$ for large value of X_F and $X = M_{\mu\mu}/\sqrt{s}$ for $X_F=0$.

4 F.W. Busser et al, Phys. Lett. 56B, 482 (1975).

5 The production of the dimuon continuum in nucleon-nucleon collisions was first reported by Christenson et al, Phys. Rev. Lett. 25, 1523 (1970).

6 S.D. Drell, T.M. Yan, Annals of Physics 66, 578 (1971); J.D. Bjorken, H. Weinberg, unpublished report to the International Conference on High Energy Physics, Palermo, Italy (1975).